

Study of the Lynx-Cancer void galaxies. - V. The extremely isolated galaxy UGC 4722

J.N. Chengalur,^{1*} S.A. Pustilnik,^{2†} D.I. Makarov,² Y.A. Perepelitsyna,²
E.S. Safonova,³ I.D. Karachentsev²

¹ *National Center for Radio Astrophysics, TIFR, Pune, India*

² *Special Astrophysical Observatory of RAS, Nizhnij Arkhyz, Karachai-Circassia 369167, Russia*

³ *Sternberg Astronomical Institute, Lomonosov Moscow State University, 13 Universitetsky pr., Moscow, 119991, Russia*

Accepted on 2014 October ?? . Received on 2014 October 2

ABSTRACT

We present a detailed study of the extremely isolated Sdm galaxy UGC 4722 ($M_B = -17.4$) located in the nearby Lynx-Cancer void. UGC 4722 is a member of the catalogue of isolated galaxies, and has also been identified as one of the most isolated galaxies in the Local Supercluster. Optical images of the galaxy however show that it has a peculiar morphology with an elongated ~ 14 kpc-long plume. New observations with the Russian 6-m telescope (BTA) and the Giant Metrewave Radio Telescope (GMRT) of the ionised and neutral gas in UGC 4722 reveal the second component responsible for the disturbed morphology of the system. This is a small, almost completely destroyed, very gas-rich dwarf ($M_B = -15.2$, $M(\text{H I})/L_B \sim 4.3$). We estimate the oxygen abundance for both galaxies to be $12 + \log(\text{O}/\text{H}) \sim 7.5 - 7.6$ which is 2–3 times lower than what is expected from the luminosity-metallicity relation for similar galaxies in denser environments. The *ugr* colours of the plume derived from Sloan Digital Sky Survey (SDSS) images are consistent with a simple stellar population with a post starburst age of 0.45–0.5 Gyr. This system hence appears to be the first known case of a minor merger with a prominent tidal feature consisting of a young stellar population.

Key words: galaxies: dwarf – galaxies: evolution – galaxies: photometry – galaxies: interactions – galaxies: individual: UGC 4722 – radio lines: galaxies – cosmology: large-scale structure of Universe

1 INTRODUCTION

Detailed studies of void galaxies allow one to determine the effect of the environment on the evolution of galaxies. The isolation and (assumed) low rate of interactions and mergers make void galaxies a useful population for testing models of galaxy formation and evolution. The possibility that galaxies in voids have significantly different properties than galaxies in denser regions has attracted considerable attention (e.g., Peebles 2001; Gottlöber et al. 2003; Hoeft et al. 2006; Hoeft and Gottlöber 2010; Hahn et al. 2007, 2009; Kreckel et al. 2011, and references therein). However, most previous studies have been focused on large distant ($d \gtrsim 100$ –200 Mpc) voids (Rojas et al. 2005; Patiri et al. 2006; Sorrentino, Antonuccio-Delogu & Rifatto 2006, among others), drawn from the SDSS and 2dFRGS surveys, and consequently are biased towards more luminous galaxies. These

studies generally found at best moderate differences between galaxies in voids and walls. Numerical simulations (e.g. Kreckel et al. 2011) predict that luminous dwarfs ($M_r \lesssim -18$) in voids are statistically indistinguishable from similar dwarfs in higher density regions. However, fainter dwarfs ($M_r \gtrsim -16$) are expected to be significantly bluer and have to have higher specific star formation rates than their higher density counterparts. Since, as mentioned above, previous studies have included very few of these faint systems, there is a clear need to extend the observational samples to include low-mass galaxies.

In order to study the effect of the environment on the properties of faint dwarfs, one would have to focus on nearby regions, where current facilities have sufficient sensitivity to detect faint dwarfs. In the surroundings of the Local Volume (i.e. the region within 10 Mpc from the Local Group) one can probe the properties of galaxies ten to hundred times less luminous than the galaxies studied in the distant voids. Motivated by this consideration

* E-mail: chengalur@ncra.tifr.res.in (JNC)

† E-mail: sap@sao.ru (SAP)

Pustilnik & Tepliakova (2011) drew up a sample of galaxies in the nearby Lynx-Cancer void. The gas phase metallicity and photometrical properties of the void galaxy population have been presented in Pustilnik, Tepliakova & Kniazev (2011); Perepelitsyna, Pustilnik, Kniazev (2014). Detailed studies of some peculiar galaxies located in this region can be found in Chengalur et al. (2006); Pustilnik et al. (2005, 2011); Chengalur & Pustilnik (2013). The galaxies studied in the last cited works are unusual in that they have a very large $M(\text{H I})/L_B$ ratio, unusually blue colours, and/or very low metallicity. Other galaxies found in nearby voids include LSBs J0015+0104 (Pustilnik et al. 2013) and J0926+3343 (Pustilnik et al. 2010) which have the 2nd and 3rd lowest metallicities known (after SBS 0335–052 W).

In this paper we present a detailed study of the Lynx-Cancer void galaxy UGC 4722. It is included in the Catalog of Isolated Galaxies (CIG) (Karachentseva 1973) as CIG 293 (KIG 293 in the nomenclature of the NASA/IPAC Extragalactic Database). The catalog was built by total visual inspection of the Palomar Sky Survey films for galaxies brighter than 15.7 mag. Karachentseva (1973) proposed the simple but effective criterion of isolation using only the angular diameters of galaxies. The isolation criteria requires the absence of ‘significant’ neighbours around the considered galaxy. We have also checked the SDSS image the region of $\pm 25'$ (roughly ± 200 kpc in projection) surrounding the galaxy, but do not find any object that could be a possible companion to this system. Finally, UGC 4722 is one of 520 galaxies identified as being the most isolated, ‘orphan’ galaxies found in the Local Supercluster (Karachentsev et al. 2011) among galaxies with known redshift. Despite being isolated UGC 4722 appears morphologically disturbed and has a long tail extending from the northern side of the disk (see Fig. 1). Karachentsev et al. (2011) listed it as one of 21 ‘orphan’ galaxies with a peculiar structure. UGC 4722 shows clear signs of interaction, but without a visible source for the disturbance. Karachentsev et al. (2006, 2008) found 8 such spatially isolated galaxies with signs of distortion, and based on the suggestions for the existence of “dark galaxies” by van den Bergh (1969) and Trentham et al. (2001), proposed that these could be cases where a galaxy is interacting with a companion consisting entirely of dark matter.

The rest of this paper is organised as follows. In Sec. 2 we describe the observations of this galaxy and the data reduction. They include H I 21-cm line observations with the GMRT (Giant Meterwave Radio Telescope) and long-slit spectra obtained using the 6-meter telescope (BTA) of the Special Astrophysical Observatory of the Russian Academy of Sciences (SAO RAS). SDSS (Sloan Digital Sky Survey) imaging data and their reduction are presented as well. In Sec. 3 we present the results of GMRT and BTA observations, as well as the result of photometry of the SDSS images. In Sec. 4 we discuss the observational properties of this unusual galaxy and discuss interpretations of the observations.

2 OBSERVATIONS AND DATA REDUCTION

2.1 Optical observations

Two long-slit spectra of UGC 4722 were obtained using the BTA and the multimode focal reducer SCORPIO in combination with grisms VPHG1200R and VPHG550G and a

2K×2K CCD detector EEV-42-40. The main observational parameters are given in Tab. 1. The observations made with the VPHG1200R grism are used for kinematical studies while the observations made with the other grism are used for abundance determinations. The slit width was $1''$, and the slit length was $\sim 6'$. Pixels along the slit were binned to give an effective pixel size of $0.36''$. The slit position (which was used for observations with both grisms) is shown in Fig. 1 superposed on the SDSS image of the UGC 4722 region (with a field size of $\sim 200''$). As can be seen from Fig. 1 the slit (labelled “1”) was aligned with the diffuse plume, and also covered the compact emission-line nebulosity ‘C’ at the northern edge of the plume as well as the bright H II-region ‘f’ at the northern end of the disk.

Archival BTA long slit observations were also available for this galaxy. The observations were taken on 18/Nov/2006 using grism VPHG1200R. The rest of the instrumental set up was identical to that described above. Observations were obtained for two slit positions, shown in Fig. 1 (labelled as “2” and “3”). As can be seen from Fig. 1, slit position 3 with a position angle of 30° is aligned with the major axis of the disk, and intersects the bright H II-regions a,b. Slit position 2 with a position angle of 13° goes along the edge of the plume. It includes the nebulosity ‘C’ at the edge of the plume and also intersects the northern edge of the disk in between the two bright H II-regions d,e.

The spectra were processed using standard procedures, as described, e.g. in Pustilnik et al. (2005). Position-Velocity (P-V) diagrams for the H α emission line were derived using a MIDAS¹ program for reduction of long-slit spectra written by Makarov and Kniazev. The details can be found in Zasov et al. (2000). For abundance determination from the spectrum with grism VPHG550G the intensities of all important emission lines were measured using standard procedures in the MIDAS package (Kniazev et al. 2008).

2.2 HI observations

GMRT H I 21 cm observations of UGC 4722 were carried out on 18/Nov/2013. The correlator was configured to a total bandwidth of 4.17 MHz (~ 890 km s^{−1}) divided into 512 channels (or a velocity resolution of 1.74 km s^{−1}) centred at the heliocentric redshift of the galaxy. The initial flagging and calibration were carried out using the FLAGCAL pipeline (Prasad & Chengalur 2012; Chengalur 2013), and the subsequent processing was done using the AIPS package. A continuum image was made using the line free channels and used for self-calibration. The self calibration solutions were then applied to the line visibilities, and the continuum emission subtracted out using the task UVSUB. Images were then made at a variety of resolutions using the task IMAGR, and residual continuum subtracted out using the task IMLIN. Images of the integrated H I emission and the H I velocity field were made using the task MOMNT.

¹ MIDAS is an acronym for the European Southern –Munich Image Data Analysis System.

[hbtp]

Table 1. Journal of the 6 m telescope observations of UGC 4722 system

Date	Expos. time [s]	Wavelength [Å]	Dispersion [Å/pixel]	Spec.resol. FWHM(Å)	Seeing [arcsec]	Airmass	Grism	Slit No.	PA (°)
(1)	(2)	(3)	(4)	(5)	(6)	(7)	(8)	(9)	(10)
2006.11.18	2×600	5700 – 7400	0.9	5.5	1.5	1.11	VPHG1200R	2	13
2006.11.18	2×600	5700 – 7400	0.9	5.5	1.5	1.08	VPHG1200R	3	30
2012.11.17	1×1200	5700 – 7400	0.9	5.5	1.7	1.06	VPHG1200R	1	4
2013.01.15	3×900	3500 – 7300	2.0	12.0	2.0	1.06	VPHG550G	1	4

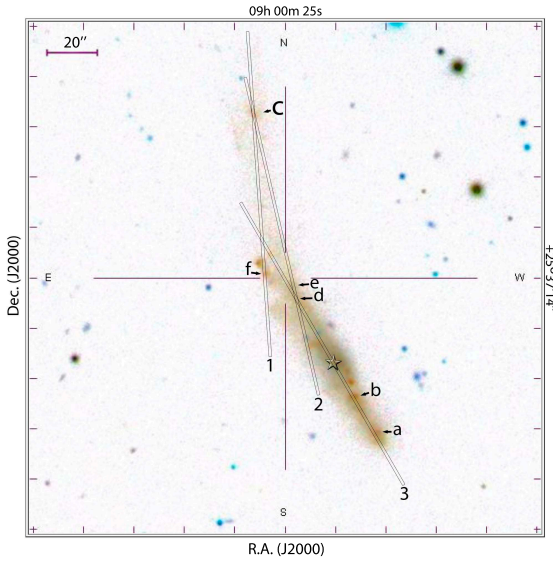


Figure 1. The SDSS *gri* image (inverse colours, size $\sim 200''$) of the system UGC 4722/UGC 4722C, with the BTA long slits shown superimposed for the observations on 18/Nov/2006 and 15/Jan/2013 (No. 1, PA = 4°) and 18/Nov/2006 (No. 2, PA = 13° and No. 3, PA = 30°). Arrows with letters indicate prominent features seen in the P–V diagrams (Fig. 2 and 3). The star shows the approximate position of the galaxy centre. This corresponds to the location of the steep velocity gradient in the P–V diagram in Fig. 3 (bottom panel).

Table 2. Parameters of the GMRT observations

	UGC 4722
Date of observations	2013 Nov 18
Field center R.A.(2000)	09 ^h 00 ^m 23.54 ^s
Field center Dec.(2000)	+25°36′40.6″
Central Velocity (km s ^{−1})	1750.0
Time on-source (h)	~6
Number of channels	256
Channel separation (km s ^{−1})	~1.73
Flux Calibrators	3C48, 3C286
Phase Calibrators	0842+185
Resolution (arcsec ²) (rms (mJy Bm ^{−1}))	41 × 38 (2.2)
	26 × 23 (1.9)
	12 × 11 (1.6)

2.3 Photometry from the SDSS images

We made photometric measurements using the public archive of the SDSS Data Release 7 (DR7; Abazajian et al. 2009). Since the SDSS provides users with fully reduced images, the only additional step we needed to perform was background subtraction. For this, all bright stars were removed from the images. After that the target object was masked and the background level was estimated using the *aip* package from MIDAS. The photometry of galaxies was then performed in circular apertures. A more detailed description of this method and the related programs can be found in Kniazev et al. (2004). To transform instrumental fluxes in apertures to stellar magnitudes, we used the photometric system coefficients defined in SDSS for the relevant fields. The accuracy of the zero-point determination was ~ 0.01 mag in all filters.

3 RESULTS

3.1 Long-slit observations

In Fig. 2 we show the H α -line intensity distribution (in relative units, solid line) along the long slit position No. 1 (top panel) and the corresponding radial velocity in km s^{−1} (bottom panel) for regions where the signal-to-noise ratio is greater than 3.0 and the error in the estimated velocity σv is less than 20 km s^{−1}. The intensity is computed within a narrow wavelength range (width $\delta\lambda = 10$ Å) centred at the redshifted H α -line. Letters ‘C’ and ‘f’ near the H α intensity peaks refer to the corresponding objects in Fig. 1. The total distance along the slit is about 110″. The left edge of the plot corresponds to the northern edge of the slit which probes the ionised gas motions in nebulosity ‘C’ at the plume edge. The size of this nebulosity is $\sim 8''$, and the slit direction is inclined at PA₁ $\sim 30^\circ$ with respect to the major axis of the nebulosity. The right edge of the plot corresponds to the NE part of the main galaxy disc with the slit direction of PA₂ $\sim 25^\circ$ with respect to the galaxy major axis.

As can be seen from the bottom panel of the figure, the velocity of the ionised gas in component ‘C’ is centred at $V_{\text{hel}}(\text{C}) \sim 1780$ km s^{−1}, and has a spread of ~ 75 km s^{−1}. The variation of velocity along the slit resembles a solid body rotation curve. For the main galaxy the velocity curve is disturbed, with a distinct velocity swing close to the position of the most prominent HII region (marked here as region ‘f’). The form and the sign of this swing is consistent with

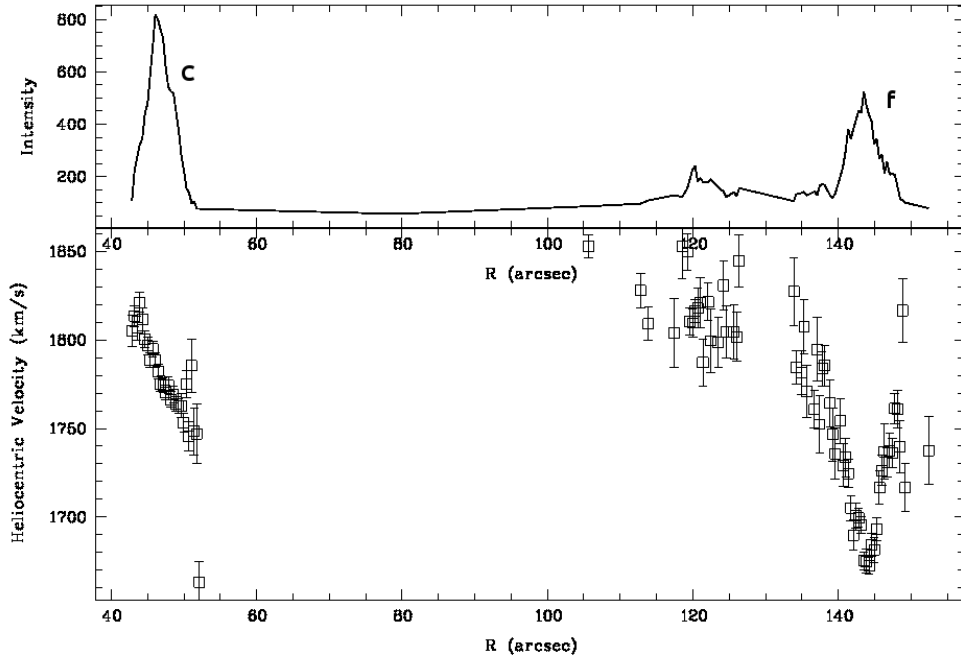


Figure 2. Slit position No. 1. Top panel: Distribution of H α -line intensity along the slit (north is in the left) in arbitrary units; Bottom panel: Position-Velocity (P-V) diagram. For both panels the X-axis shows the position along the slit in arcsec. The Y-axis shows the relative intensities and radial velocity in km s^{-1} respectively. Letters ‘C’ and ‘f’ on H α intensity peaks denote to corresponding objects in Fig. 1

it arising from an expanding ionised shell around the off-plane HII region with maximal velocities of $\sim 60\text{--}80 \text{ km s}^{-1}$. Similar cases of expanding H α shells were presented for e.g. in Pustilnik et al. (2003); physical models for these shells are discussed by Walter & Brinks (1999). The ionised gas outside of the shell has a velocity of $\sim 1810 \text{ km s}^{-1}$, with a spread of $\pm 20\text{--}30 \text{ km s}^{-1}$.

In Fig. 3 we present similar data for observations from the BTA run on 18/Nov/2006. In the top panel we show the distribution of the H α intensity and radial velocity for slit position No. 2 (along the northern part of the main galaxy disc, plume and component ‘C’). The positions of the prominent HII-regions ‘C’, ‘d’ and ‘f’ are also marked. Similar velocity swings with amplitudes of $30\text{--}40 \text{ km s}^{-1}$ are seen near the latter two regions. For component ‘C’ the ‘solid-body’ like rotation is seen with full amplitude range of $\sim 60 \text{ km s}^{-1}$. In the bottom panel similar data are shown for slit position No. 3 (i.e. along the main galaxy major axis). There are several prominent HII-regions in the southern part of the disc (including ‘a’ and ‘b’), and smaller regions in the northern part, including ‘d’ on the edge. The velocity curve shows a steep gradient near the centre of the galaxy (i.e. abscissa between 190 and 195), which flattens as one approaches the edge of the visible H α extent of the galaxy (i.e. $\sim 95''$). As in the previous plots, multiple velocity swings are seen near positions of prominent HII-regions, indicative of expanding shells. Accounting for these swings, the total rotation velocity amplitude is $\sim 130 \text{ km s}^{-1}$ somewhat smaller than the velocity spread seen in the H I (see Sec. 3.2 below). We also

note that the H α velocities for the central part of UGC 4722 appear to suffer from a systematic zero-point shift of $\sim 20\text{--}30 \text{ km s}^{-1}$ with respect to the H I velocities described below. This systematic error is within the expected internal velocity calibration error for the optical long slit spectra.

3.2 H I distribution and velocity field

The integrated H I maps at different resolutions ($\sim 40''$, $25''$, and $12''$) are shown superimposed on the SDSS g -filter image in Figs. 4, 5 and 6. From the figures it appears clear that this system consists of two interacting galaxies, with an H I-bridge connecting them. This bridge coincides with the optical plume and the H I concentration corresponds to the nebulousity ‘C’ at the end of the plume. In the higher resolution images, one can see that the peak of the H I emission is slightly offset from the location of the optical nebulousity. The plume (or bridge connecting both galaxies) most probably consists of material pulled out from the smaller component. We denote this second galaxy as UGC 4722C. The H I-velocity field at resolutions of $\sim 40''$ and $12''$ are shown in Figures 4, 6. At the higher resolution there is a hint that the kinematical major axis of H I-gas near component ‘C’ is perpendicular to the kinematical major axis of the main galaxy. We note that another possible interpretation is for component ‘C’ to be a tidal dwarf galaxy, with the tidal features being produced by the gravitational interaction of UGC 4722 with an unseen dark galaxy. While this

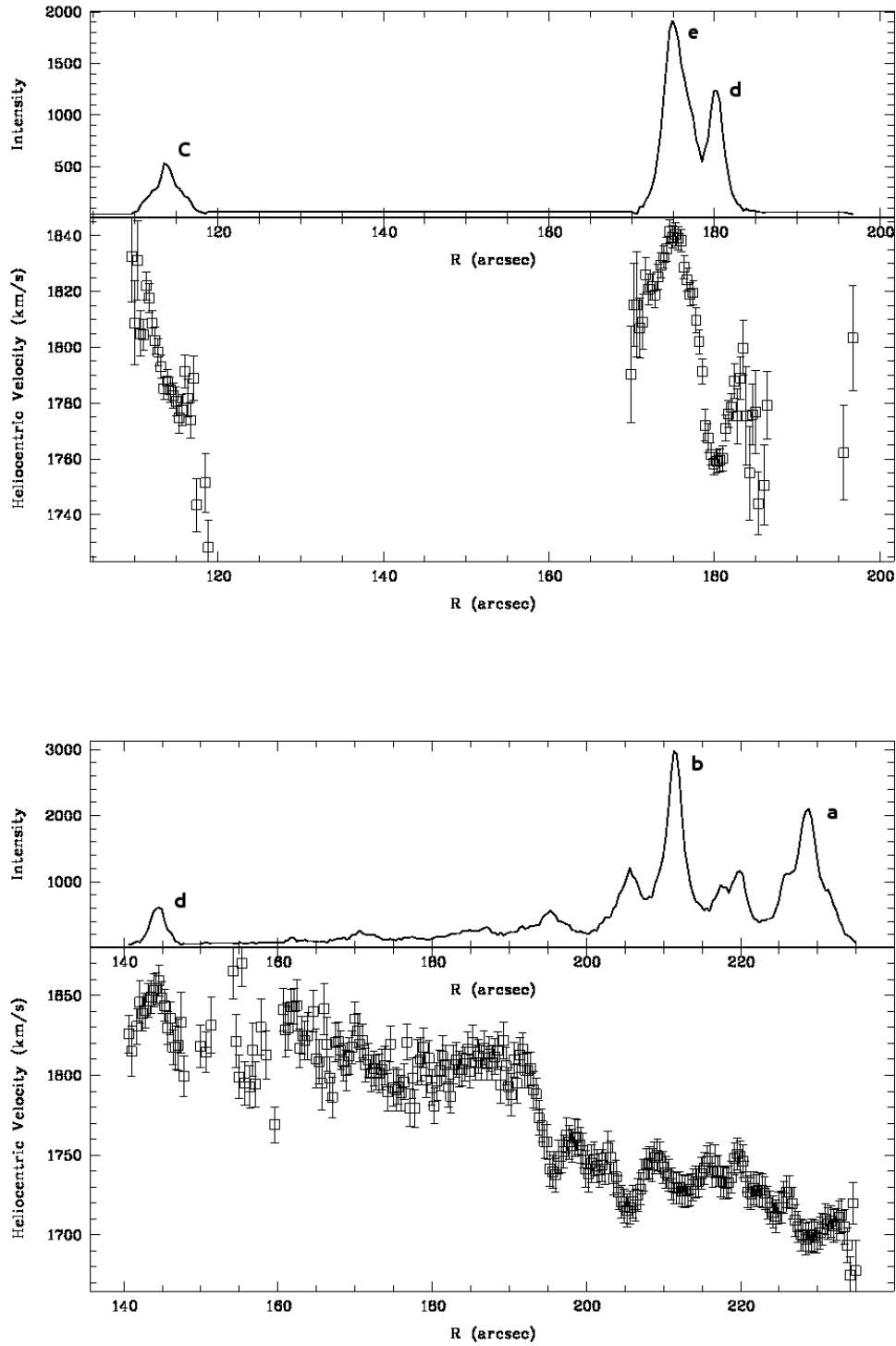


Figure 3. Same as in Fig. 2, but for observations on 18/Nov/2006. Top panel: Slit position No. 2. The distribution of H α intensity (arbitrary units) and the P-V diagram. The compact nebulosity 'C' is centered at $X \sim 114''$. Bottom panel: Slit position No. 3. Letters 'C', 'a' - 'e' on the H α intensity peaks refer to the corresponding objects in Fig. 1.

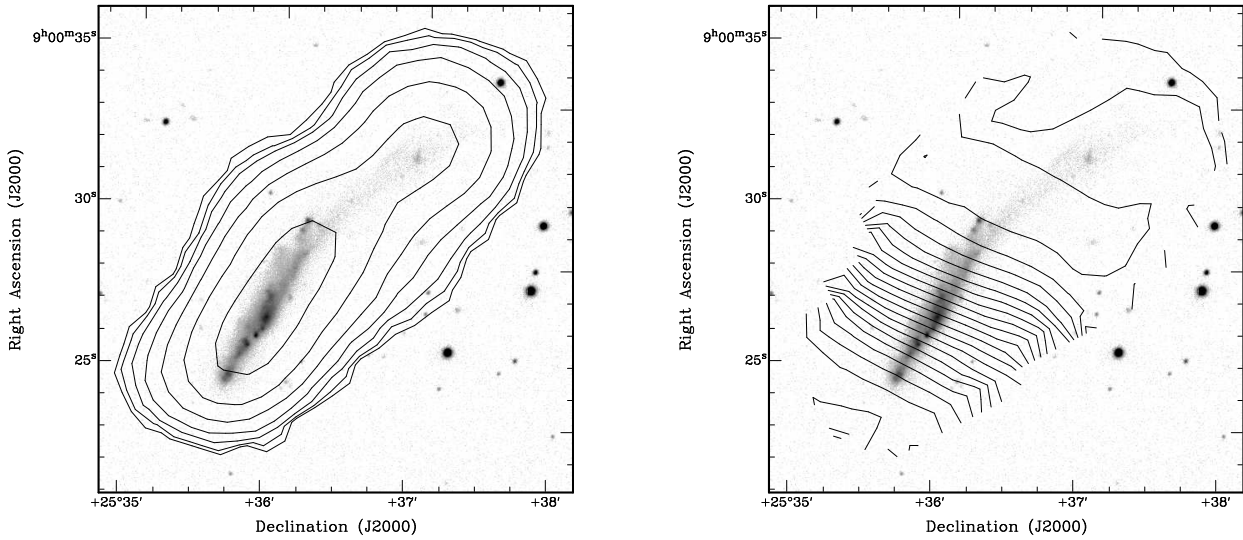


Figure 4. **Left panel:** Integrated HI emission from the UGC 4722 system at a resolution of $\sim 40''$ (contours) overlaid on the SDSS *g*-band image (greyscales). The contours start at 2.5×10^{19} atoms cm^{-2} and are spaced a factor of 2 apart. **Right panel:** similar map, but for the velocity field. The iso velocity contours start at 1735 km s^{-1} and are spaced 5 km s^{-1} apart. The velocity increases smoothly from the SW to the NE.

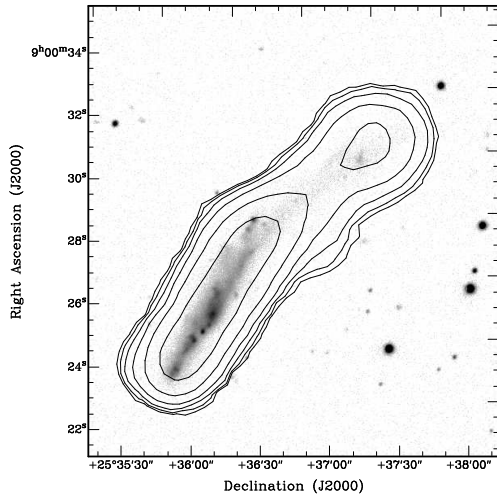


Figure 5. Integrated HI emission from the UGC 4722 system (contours) at a resolution of $\sim 25''$ overlaid on the SDSS *g*-band image (greyscales). The HI contours start at 6×10^{19} atoms cm^{-2} and are spaced a factor of 2 apart.

possibility cannot be ruled out without detailed numerical simulations, a more straight forward explanation is what is proposed above, i.e. that the system consists of a pair of merging dwarf galaxies.

The integrated HI-profile (at $40''$ resolution) of UGC 4722 is shown in Fig. 7, along with the profile for the main galaxy disk and the profile of the plume. The total integrated flux measured from this profile is $12.1 \pm 1.0 \text{ Jy km s}^{-1}$, which is about $\sim 87\%$ of the single dish flux measured by the Arecibo Telescope (Haynes et al., 2011). The quoted error bar includes the uncertainty in the absolute flux calibration. From a comparison of the GMRT and Arecibo profiles (not shown), it appears that some gas near the average velocity of

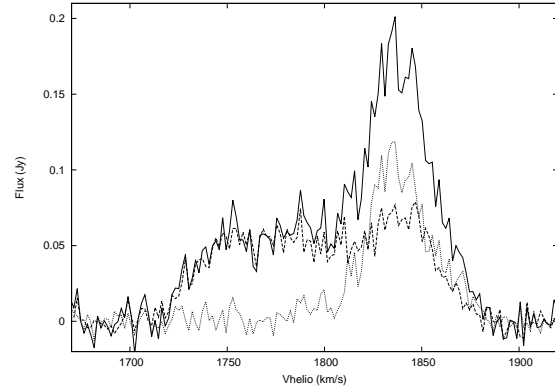


Figure 7. The integrated HI-profile of UGC 4722 obtained from $40''$ resolution datacube (solid line). Also shown are the integrated spectrum of the region corresponding to the disk of the main galaxy (dashed line) and the integrated spectrum of the plume (dotted line).

the system has been resolved out. For the main galaxy disk the integrated HI flux is 7.6 Jy km s^{-1} , the central velocity is $1795 \pm 3 \text{ km s}^{-1}$ and the velocity widths at the 50% and 20% levels are $W_{50} = 130 \pm 3 \text{ km s}^{-1}$, $W_{20} = 150 \pm 3 \text{ km s}^{-1}$. For the plume the corresponding quantities are 4.3 Jy km s^{-1} , $V_{\text{helio}} = 1837 \pm 3 \text{ km s}^{-1}$ and $W_{50} \sim 38 \pm 3 \text{ km s}^{-1}$. In case that most of the emission resolved-out in the GMRT observations relates to the main disc, its HI flux can be as large as to 9.6 Jy km s^{-1} . Its total mass $M(\text{HI})$ and $M(\text{HI})/L_B$ ratio would then be $\sim 25\%$ larger than what is listed in Tab. 6.

3.3 Photometric properties

The photometric parameters measured from the SDSS images are given in Table 3. The table contains the measured total magnitudes g_{tot} , colours $(u - g)$, $(g - r)$ and $(r - i)$,

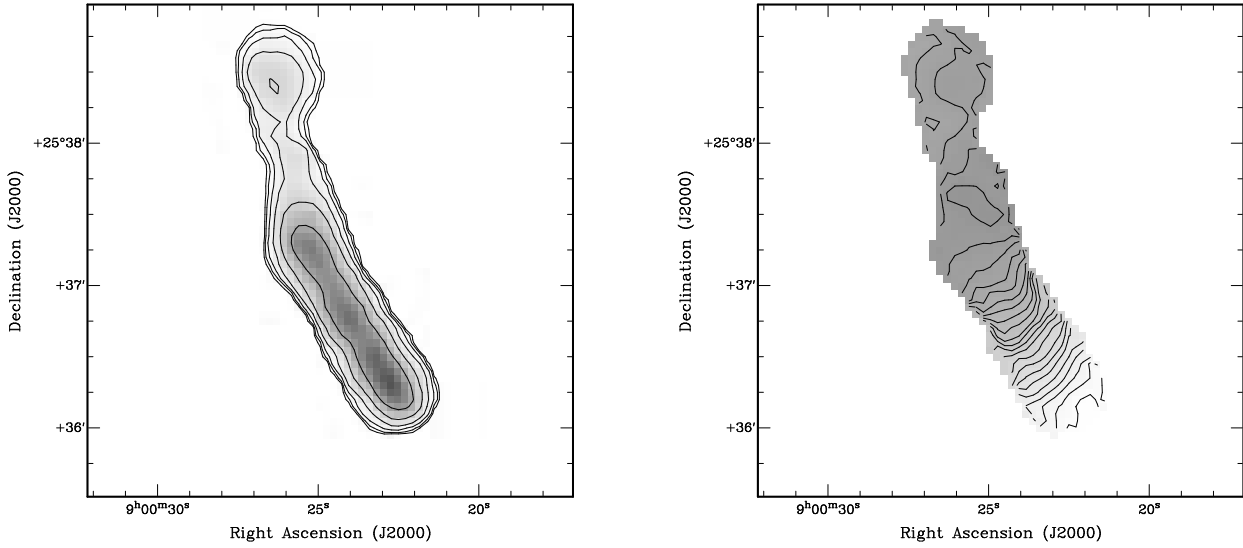


Figure 6. **Left panel:** Integrated HI emission for a beamwidth of $12''$ (both contours and greyscales). The contour levels start at $1 \times 10^{20} \text{ atoms cm}^{-2}$, and are spaced apart by a factor of 2. **Right panel:** HI velocity field at a resolution of $12''$. The contours start at 1750 km s^{-1} and are spaced 5 km s^{-1} apart.

Table 3. Photometric parameters of UGC 4722, UGC 4722C and the Plume

Parameter	UGC 4722	UGC 4722C	Plume
g_{tot}	14.70 ± 0.01	19.26 ± 0.02	16.94 ± 0.01
$(u - g)_{\text{tot}}$	0.96 ± 0.01	0.56 ± 0.05	1.08 ± 0.03
$(g - r)_{\text{tot}}$	0.25 ± 0.01	0.11 ± 0.03	0.13 ± 0.01
$(r - i)_{\text{tot}}$	0.10 ± 0.01	-0.15 ± 0.04	0.09 ± 0.02
$(u - g)_{\text{tot},0}$	0.91 ± 0.01	0.51 ± 0.05	1.03 ± 0.03
$(g - r)_{\text{tot},0}$	0.20 ± 0.01	0.06 ± 0.03	0.08 ± 0.01
$(r - i)_{\text{tot},0}$	0.08 ± 0.01	-0.17 ± 0.04	0.07 ± 0.02
B_{tot}	15.01 ± 0.02	19.53 ± 0.03	17.21 ± 0.02
$(b/a)_{25}$	0.22	0.50	—
$\mu_g (\text{mag arcsec}^{-2})$	24.04 ± 0.28	25.20 ± 0.02	24.80
$\mu_r (\text{mag arcsec}^{-2})$	24.40 ± 0.15	24.99 ± 0.02	24.60
$\mu_B (\text{mag arcsec}^{-2})$	24.15 ± 0.32	25.50 ± 0.02	25.10
$\mu_{B,c,i} (\text{mag arcsec}^{-2})$	24.47 ± 0.32	—	—
$n_g (\text{Sersic})$	1.23 ± 0.24	—	—
$\alpha_g (")$	7.3 ± 1.8	—	—

(1) – values of the total magnitudes are not corrected for the MW foreground extinction; (2) – for UGC 4722, μ corresponds to the central brightness of the model disc $\mu_{0,g}$ (see Paper IV), while for UGC 4722C – to the effective surface brightness $\mu_{\text{eff},g}$ – a mean within the effective radius, and for the plume to that within a circular aperture with $R=7.9''$.

the derived B_{tot} , as well as the axial ratio b/a for the both galaxies. Also we show the total magnitude of the plume emission, the derived central surface brightness in g and r filters for UGC 4722, the corresponding central brightness in B , transformed using the formulae given in Lupton et al. (2006), as well as this parameter corrected for the Milky Way extinction (Schlafly & Finkbeiner 2011) and inclination. Finally, the model fit parameters for UGC 4722 are included: the Sersic profile index and its characteristic radius.

For component ‘C’ and the total emission of ‘plume+C’

Table 4. Line intensities in spectra of UGC 4722 and UGC 4722C

$\lambda_0 (\text{\AA})$ Ion	UGC 4722 ‘f’		UGC 4722C	
	$F/F(\text{H}\beta)$	$I/I(\text{H}\beta)$	$F/F(\text{H}\beta)$	$I/I(\text{H}\beta)$
3727 [O II]	3.75 ± 0.79	2.71 ± 0.82	4.10 ± 0.30	4.15 ± 0.35
4340 H γ	0.14 ± 0.06	0.42 ± 0.45	0.34 ± 0.03	0.47 ± 0.05
4861 H β	1.00 ± 0.20	1.00 ± 0.37	1.00 ± 0.06	1.00 ± 0.07
4959 [O III]	1.18 ± 0.22	0.86 ± 0.22	0.25 ± 0.04	0.23 ± 0.04
5007 [O III]	2.69 ± 0.40	1.95 ± 0.40	0.82 ± 0.07	0.73 ± 0.07
6548 [N II]	0.02 ± 0.03	0.01 ± 0.03	0.05 ± 0.03	0.04 ± 0.02
6563 H α	3.61 ± 0.51	2.78 ± 0.61	3.45 ± 0.16	2.78 ± 0.16
6584 [N II]	0.09 ± 0.05	0.07 ± 0.05	0.20 ± 0.04	0.16 ± 0.03
6716 [S II]	0.46 ± 0.09	0.33 ± 0.09	0.51 ± 0.05	0.40 ± 0.04
6730 [S II]	0.32 ± 0.08	0.23 ± 0.08	0.36 ± 0.05	0.28 ± 0.04
C(H β) dex	0.00 ± 0.18		0.16 ± 0.06	
EW(abs) \AA	3.50 ± 2.25		3.7 ± 0.31	
$F(\text{H}\beta)^a$	0.65 ± 0.09		2.29 ± 0.09	
EW(H β) \AA	9.12 ± 1.26		33.88 ± 1.55	
V_{hel} km s^{-1}	1860 ± 42		1830 ± 54	

^a in units of $10^{-16} \text{ ergs s}^{-1} \text{ cm}^{-2}$.

the surface brightness relates to model-independent parameters, since it is rather difficult to apply models to their surface brightness distributions. Thus, for ‘C’ the μ_{eff} in filters g, r, B refers to the mean within the effective radius, while for the plume this is simply the mean within a circular aperture with $R=7.9''$.

3.4 Oxygen abundances

After processing the long-slit spectrum, described in Sec. 2 (No. 1, grism VPHG550G), we obtained a 2D spectrum, from which we extracted for further analysis two 1D spectra with the largest signal-to-noise ratio for the strong emission lines. This was done using standard techniques

Table 5. Derived physical parameters and Oxygen abundances

Value	UGC 4722 ‘f’	UGC 4722C
$T_e(\text{OIII})(10^3 \text{ K})$	16.11 ± 1.86	16.56 ± 1.13
$T_e(\text{OII})(10^3 \text{ K})$	14.39 ± 1.98	14.54 ± 1.19
$N_e(\text{SII})(\text{cm}^{-3})$	10 ± 10	10 ± 10
$\text{O}^+/\text{H}^+(\times 10^{-4})$	0.280 ± 0.149	0.414 ± 0.113
$\text{O}^{++}/\text{H}^+(\times 10^{-4})$	0.193 ± 0.062	0.062 ± 0.011
$\text{O}/\text{H}(\times 10^{-4})$	0.474 ± 0.162	0.476 ± 0.113
$12+\log(\text{O}/\text{H}) \text{ (IT07)}$	7.68 ± 0.15	7.68 ± 0.10
$12+\log(\text{O}/\text{H}) \text{ (PM2010)}$	7.59 ± 0.21	7.42 ± 0.10
$12+\log(\text{O}/\text{H}) \text{ (weigh. mean)}$	7.64 ± 0.06	7.50 ± 0.10

(see e.g., Kniazev et al. 2008, for a detailed description). In Fig. 8 (top) we show the extracted 1D spectrum for the brightest central part (extent $\sim 1.8''$) of the prominent HII-region in UGC 4722 (region ‘f’), while in Fig. 8 (bottom) we show the extracted 1D spectrum for the brightest central part of the faint nebula ‘C’ (extent $\sim 3.2''$). The measured line intensities, used for determination of the oxygen abundance O/H are listed in the upper part of Table 4. In the bottom of the Table we also give the derived parameters of the extinction coefficient $C(\text{H}\beta)$, the equivalent width of the Balmer absorption ($\text{EW}(\text{abs})$), the total flux in the $\text{H}\beta$ line, the equivalent width of the $\text{H}\beta$ emission ($\text{EW}(\text{H}\beta)$) and the weighted value of the radial velocity, derived from redshifts of strong emission lines.

Both the spectra are rather noisy, so it was possible to measure fluxes only for the strongest emission lines. In particular, given the modest signal-to-noise and equivalent widths of $[\text{OIII}]\lambda 4959$ line, it is understandable that we do not detect the temperature-sensitive $[\text{OIII}]\lambda 4363$ line, which is normally a factor of 12 to 30 times fainter in the T_e range of 20000 K to 13000 K. We are hence unable to use the classical T_e method to estimate O/H from these spectra. Instead we used the well-calibrated and reliable semi-empirical method of Izotov & Thuan (2007) as well as the empirical estimator suggested by Pilyugin & Mattsson (2011), both of which use only the intensities of the strong lines.

The resulting physical parameters and the derived values of O/H with their errors are given in Table 5. The parameters listed include the electron temperature in the main O^{++} emission zone, $T_e(\text{OIII})$ (derived via the semi-empirical method), the temperature in the O^+ zone, $T_e(\text{OII})$, and the adopted value of the electron density N_e . The derived relative abundances of O^+ , O^{++} and O along with their errors are shown in the next three entries. Finally, we show the parameter $12+\log(\text{O}/\text{H})$ derived via semi-empirical method as well as with empirical O/H estimator of Pilyugin & Mattsson (2011). We also calculated the weighted mean of these two values, which we use for all further analysis below.

4 DISCUSSION

As discussed above, UGC 4722 is located in the nearby Lynx-Cancer void and is one of the most isolated galaxies known. It is a member of both the Catalogue of Isolated Galaxies (CIG) as well as the AMIGA sample of iso-

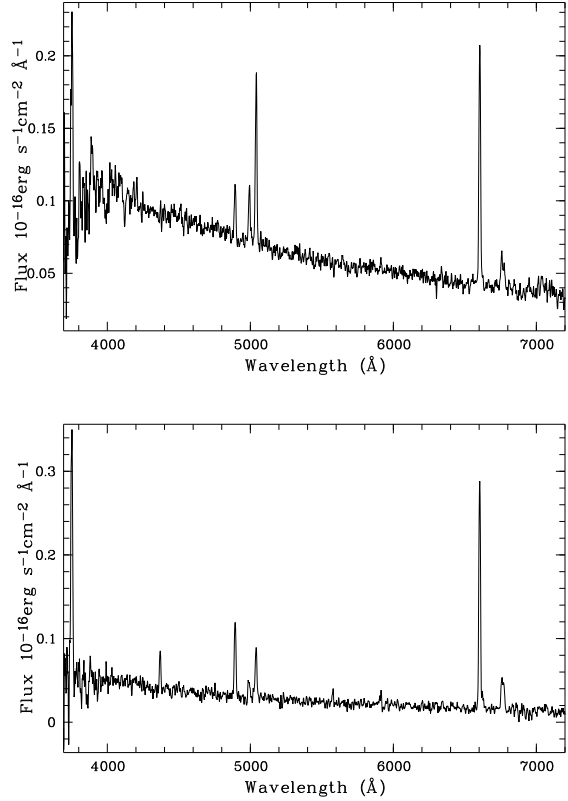


Figure 8. The BTA mid-resolution spectra of UGC 4722 system (see regions in Fig. 1). Top panel: 1D-spectrum of the bright HII-region on the northern edge of UGC 4722 (region ‘f’). Bottom panel: 1D-spectrum of the nebula ‘C’.

lated galaxies. Our HI and optical data however suggest that this system actually consists of a pair of interacting dwarf galaxies. This indicates that the selection criteria for these samples of isolated galaxies allow at least some minor merger type systems to be classified as isolated galaxies. The finding that UGC 4722 consists of a galaxy pair, as well as the other discovery of pairs and small groups of dwarf galaxies in nearby voids is also consistent with the suggestion of Kreckel et al. (2012) that the small scale clustering in voids is similar to that in the general field Karachentsev & Makarov (2008); Makarov & Karachentsev (2009). Below we discuss in the detailed properties of the UGC 4722 system.

4.1 Main parameters

In Table 6 we present the main parameters of the UGC 4722 system. From the total magnitudes in the g and r filters (Table 3) and the transformation equations between SDSS magnitudes and other systems by Lupton², we derived the total B -band magnitudes, $B_{\text{tot}} = 15.01 \pm 0.02$ and 19.53 ± 0.03 for the main galaxy and the nebula ‘C’ respectively. As mentioned above, we assume that the plume consists of material pulled out from the fainter galaxy. It is then natural

² <https://www.sdss3.org/dr8/algorithms/sdssUBVRITransform.php#Lupton2005>

to add the integrated light of the plume to that of the nebula 'C' itself, in order to get a robust estimate of the total luminosity of the companion. These total magnitudes, designated as C+plume, are also listed.

Following Pustilnik & Tepliakova (2011) in assuming that this system has a large peculiar velocity (as suggested earlier by Tully et al. (2008)), we adopt its distance modulus of $\mu=32.22$ ($D=27.8$ Mpc). We note that the distance adopted here is close to the average value of 26.2 Mpc listed in NED (which is derived from the Tully-Fisher relation). The corresponding absolute magnitudes are hence $M_B^0 = -17.38$ (main galaxy), -12.86 (nebula 'C') and -15.18 ('C' + plume). This implies that the ratio of blue luminosities of the two interacting galaxies is ~ 7.7 (in contrast to the ratio of $M(\text{H}\alpha)\sim 1.8$). The $M(\text{H}\alpha)/L_B$ ratio (in solar units) for the galaxies is ~ 1.0 for the main galaxy and ~ 4.3 for 'C'+plume. The estimate of the minimal dynamical mass of the main disc UGC 4722, adopting its distance, H α -radius of $50''$ and $V_{\text{rot}}=75 \text{ km s}^{-1}$ (i.e. half of the 20% width W_{20}) gives the value of $M_{\text{dyn}}(\text{UGC 4722}) \sim 8.5 \times 10^9 M_\odot$. For component 'C' both because of the highly disturbed nature of the velocity field, as well as the fragmented nature of the object we are unable to estimate the dynamical mass.

4.2 Plume properties

To better understand the properties of the plume, we examine the SDSS-based surface brightness, magnitudes, colours and their gradients along the plume. The *ugri* colours do not show visible gradients along the plume. Therefore it is reasonable to work with the integrated plume parameters. The integrated *ugri* colours, (after accounting for the Galaxy foreground extinction (Schlafly & Finkbeiner 2011)) are as follows: $(u - g)_0 = 1.03 \pm 0.03$, $(g - r)_0 = 0.08 \pm 0.01$, $(r - i)_0 = 0.07 \pm 0.02$.

As can be seen in Fig. 9, these colours are an excellent match to the PEGASE2 (Fioc & Rocca-Volmerange 1999) evolutionary model tracks for instantaneous SF (or simple stellar population, SSP) for both Salpeter (1955) and Kroupa et al. (1993) Initial Mass Functions (IMF) and metallicity $z=0.002$ (roughly $Z = Z_\odot/10$). The latter Z is close to the metallicity found in the central HII-region of the nebula 'C'. The tracks for both types of IMF run very close to each other at this time range (around 0.5 Gyr). Our best fit estimate of the time since the starburst corresponds to $\sim 0.45\text{--}0.5$ Gyr with a Salpeter IMF. Observational studies show that the peak in star formation activity in companion galaxies occurs near the pericenter passage (e.g. Patton et al. (2013). Numerical models (e.g., GalMer, Di Matteo et al. (2008)) also make similar predictions, albeit for specific initial conditions. Our estimated star burst time hence corresponds approximately to the time since the last close encounter between the two galaxies. This in turn allows us to estimate the relative velocity of the companion in the sky plane. Dividing the projected distance between the centres of UGC 4722 and the nebula 'C' (i.e. ~ 13.8 kpc) by the time since perigalactic passage (i.e. ~ 500 Myr), one obtains $V_{\text{trans}} \sim 28 \text{ km s}^{-1}$. This is about 0.6 of the difference in radial velocities between the two components.

From the PEGASE2 models one can derive many parameters related to the stellar population including the

temporal dependence of the specific luminosity (per solar mass) in several passbands. Adopting these parameters at an epoch of $T=500$ Myr, as well as the solar absolute magnitude of $M_V=3.78$ and the colour index $g - V=-0.11$, we get $M_g=3.67$. For the estimated plume absolute magnitude $M_{g,\text{plume}}=-15.38$, one then derives a total stellar mass of $4.6 \times 10^7 M_\odot$. This can be compared to the total H α -mass ($M(\text{H}\alpha)=78 \times 10^7 M_\odot$) or a total gas mass ($M(\text{H}\alpha+\text{He})=1.33 \times M(\text{H}\alpha)$), $M_{\text{gas}} = 104 \times 10^7 M_\odot$. That is the plume's visible stellar mass comprises only $\sim 4\%$ of its baryonic mass.

4.3 Gas Phase metallicities

We obtained two O/H measurements in this system: one in the central HII-region of the nebula 'C' and the second - in the bright HII-region on the edge of the UGC 4722 disk (region 'f'). Both the measured values are rather similar, with the formal difference (~ 0.08 dex) being comparable to the uncertainties (~ 0.07 and 0.12 dex). We note that differences in O/H of as large as $\sim 0.25\text{--}0.30$ dex (i.e. up to factor of two) would be consistent with our error bars. Significantly higher S/N-ratio spectra of these HII regions would be needed to rule out this possibility.

We also checked whether these measured metallicities are consistent with the luminosity-metallicity ("L-Z") relation derived for galaxies residing in denser environments. In particular, we compare their metallicities with that expected from the relation derived for the Local Volume dwarfs with well-known distances and O/H by Berg et al. (2012). The scatter in this relation is quite small, $\sigma_{(\text{O}/\text{H})}=0.15$ dex. The comparison shows that the measured O/H in our two dwarfs are lower than what would be expected from the L-Z relation by a factor of ~ 3 for the main galaxy UGC 4722 and a factor of ~ 2 for the smaller companion UGC 4722C. The deviation is significantly larger than the measurement errors. While this deviation may partly result from gas infall from the 'unevolved' outer parts of the galaxies due to the strong tidal disturbance (as suggested by Ekta & Chengalur 2010; Montuori et al. 2010), we also note that galaxies in the Lynx-Cancer void in general have a lower value (by $\sim 30\text{--}50\%$) of O/H, (Pustilnik, Tepliakova & Kniazev 2011) than galaxies residing in denser regions.

4.4 Origin of UGC 4722 and comparison with other similar systems

The suggestion in Karachentsev et al. (2008) that the UGC4722 system represents the interaction between a dwarf galaxy and a "dark" galaxy now appears unlikely, since the baryonic mass in the plume ($\sim 10^8 M_\odot$) is larger than the mass of the 'dark' halos expected in the LCDM models. Instead, a plausible scenario for the UGC4722C system is that it is the result of a minor merger between UGC4722 and an extremely gas rich companion which has come in on a parabolic orbit. Had the companion been on a bound orbit, one would have expected that the extended tidal interaction could have led either to a disruption of the galaxy or that tidally induced star formation would have led to a larger stellar mass fraction. After the closest approach of the parabolic orbit ~ 0.5 Gyr ago, some of the gas ($\sim 4\%$)

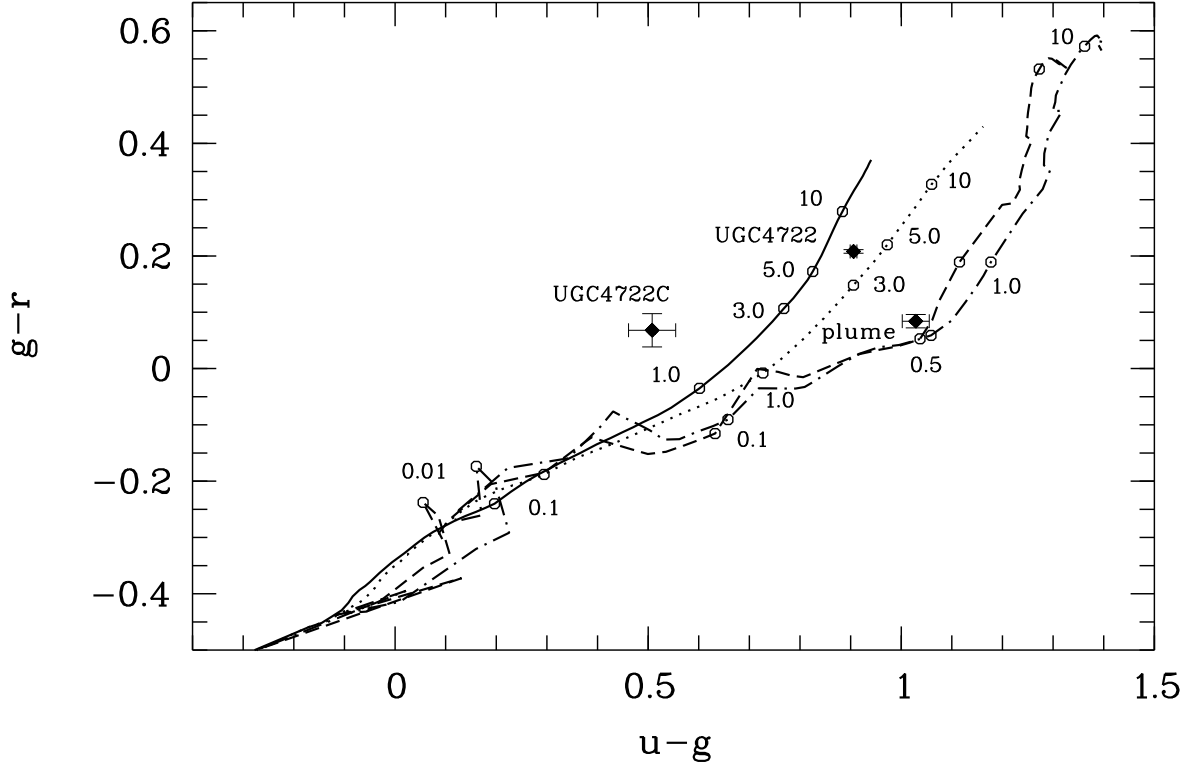


Figure 9. PEGASE2 evolutionary tracks for constant SFR and instantaneous SF and metallicity of $z=0.002$. Solid line corresponds constant SFR with Salpeter (1955) IMF; dot – constant SFR with Kroupa et al. (1993) IMF; dash – instantaneous SF with Salpeter IMF; dot-dash – instantaneous SF with Kroupa IMF. Octagons along the tracks (with corresponding numbers) mark the time elapsed since the beginning of SF (in Gyr). The integrated colours corrected for Galactic extinction are shown by black diamonds with error bars and are marked by object names (UGC 4722 – the main Sdm galaxy, UGC 4722C – compact emission-line nebulosity at the plume edge, plume – total emission of the plume and nebulosity ‘C’). See Sec. 4 for details. We note that the colours of nebulosity ‘C’ are affected by the nebular emission related to its recent and current SF activity, however it has negligible effect on the integrated colours of the plume.

collapsed and transformed to stars while a significant fraction of the gas was also pulled out to form the “plume”. In this scenario it is interesting to try and determine what the properties of the smaller companion galaxy were before the start of the collision. From the currently available optical data, it is difficult to estimate the mass of the stellar population of the companion with ages older than 1 Gyr. If there were to be such a population, one would expect that it could also be pulled out in the plume but would remain undetectable because of its very low surface brightness. It seems reasonable to assume however that any such population would have a stellar mass similar to that of the stellar mass of the ‘old’ stellar population related to UGC 4722C, which is ~ 7 times less luminous than the plume. This implies that before the collision the companion was an extremely gas-rich dwarf. In the most extreme case, when the most of its stars formed in the course of the current collision, the pre-collision stellar mass fraction could be as low as 1% or smaller. While this is indeed unusual, it would not be a unique case, as several similar very gas-rich dwarfs have already found in this void (Pustilnik et al. 2011). In fact the Lynx-Cancer void hosts two even more extreme gas-rich dwarfs (Chengalur & Pustilnik 2013). An alternative model to the minor merger is that the UGC4722 represents a

very clumpy gas disk. While the disks of somewhat brighter gas rich galaxies are known to be somewhat clumpy (e.g. Wang et al. 2013)), cases as disturbed looking as UGC4722 are rare. Additionally, the kinematics of the UGC4722 system are clearly discrepant from what one would expect from a clumpy disk.

The only similar morphology galaxy which we found in the literature is DDO 169 (UGC 8331). This is a nearby dwarf irregular galaxy ($M_B \sim -13.8$, $D_{\text{TRGB}}=4.4$ Mpc), which has been used in many statistical studies. The only detailed paper dedicated to this galaxy by Iyer & Simpson (2007) is based on rather shallow HI VLA observations (10 and 20 minutes of integration in C and D configurations) and H α imaging. The earlier HI-maps obtained with Westerbork Radio Telescope also provide only limited sensitivity³. Iyer & Simpson (2007) did not measure the colours of the plume, or those of the brighter knots on the plume edge, and detected H α emission only near the bright central body of the galaxy. In the VLA maps one can see that there is a HI-peak that coincides with an optical knot at the end of the plume. UGC 8331 and UGC 4722 hence appear fairly similar, but a more detailed study of UGC 8331

³ <http://www.nrao.edu/astrores/HIroques/>

Table 6. Main parameters of UGC 4722 and UGC 4722C

Parameter	UGC 4722	UGC 4722C
R.A.(J2000.0)	09 00 23.54	09 00 26.11
DEC.(J2000.0)	+25 36 40.6	+25 38 21.4
A_B (from NED)	0.17	0.17
B_{tot}	15.01 ⁽¹⁾	19.53 ⁽¹⁾
B_{tot}		17.21 (C+Plume)
$V_{\text{hel}}(\text{HI})(\text{km s}^{-1})$	1795±1 ⁽¹⁾	1837±4 ⁽¹⁾
$V_{\text{hel}}(\text{opt})(\text{km s}^{-1})$	1780±5 ⁽¹⁾	1795±5 ⁽¹⁾
$V_{\text{LG}}(\text{opt})(\text{km s}^{-1})$	1714	1729
Distance (Mpc)	27.8 ⁽¹⁾	27.8 ⁽¹⁾
M_B^0	-17.38 ⁽¹⁾	-12.86 ⁽¹⁾
M_B^0		-15.18 (C+Plume)
Opt. size (″) ⁽⁵⁾	90×20 ⁽¹⁾	10×5 ⁽¹⁾
Opt. size (kpc)	12.1×2.7	1.35×0.67
$\mu_{B,c,i}^0(\text{mag arcsec}^{-2})$	23.35 ⁽¹⁾	—
12+log(O/H)	7.64±0.06 ⁽¹⁾	7.50±0.10 ⁽¹⁾
HI int.flux ⁽⁶⁾	7.6±1.2 ⁽²⁾	4.3±0.2 ⁽²⁾
$W_{50}(\text{km s}^{-1})$	130±3 ⁽²⁾	38±3 ⁽²⁾
$V_{\text{rot}}(\text{km s}^{-1})$	75 ⁽³⁾	43 ⁽⁴⁾
$M(\text{HI})(10^7 M_{\odot})$	138 ⁽¹⁾	78 ⁽¹⁾
$M_{\text{dyn}}(10^8 M_{\odot})$	85 ⁽¹⁾	—
$M(\text{HI})/L_B^{(7)}$	1.0 ⁽¹⁾	4.3 ⁽¹⁾

(1) – derived in this paper; (2) – derived from the GMRT HI-profile. Real HI-flux and mass of UGC 4722 can be ~25% larger; (3) – derived from the GMRT HI-profile and (4) – from H α P–V diagram (UGC 4722C); (5) – $a \times b$ at $\mu_B = 25^{\text{m}}0 \text{ arcsec}^{-2}$; (6) – in units of Jy·km s⁻¹; (7) – in solar units.

will be needed to establish this in detail. There are also two other objects with tidal tails/plumes that resemble the UGC 4722 system. One of the best known is the Tadpole galaxy (UGC 10214=VV 29), studied in detail by Briggs et al. (2001). Several very LSB plumes near large disc galaxies are found by Miskolczi, Bomans & Dettmar (2011) via deep analysis of the SDSS images. Some of them can be analogs of UGC 4722 case.

Although the number of such objects known appears limited, we note that the UGC 4722 system has many similarities with other small dwarf aggregates found in voids. Like UGC 4722, many void pair and triplet members, show elevated values of $M(\text{HI})/L_B$ (~2 to 25), blue colours of their outer regions and low O/H. Examples include: the merger remnant/triplet DDO 68 (Ekta, Chengalur, Pustilnik 2008; Tikhonov et al. 2014; Cannon et al. 2014), the triplet J0723+36 (Chengalur & Pustilnik 2013), the pair HS 0822+3542/SAO 0822+3545 (Chengalur et al. 2006), pair J0852+13 and the triplet MRK 407 (Chengalur et al., in prep.). A more detailed comparison of these unusual systems in voids is postponed to the separate paper. We also note that there are very few detailed numerical simulations of the merger of extremely gas rich small systems. Such studies would be an important theoretical counterpart to the observations of UGC 4722 and the other systems discussed above. Understanding the merger of small gas rich objects is also important to a more detailed understanding of hierarchical galaxy formation models.

5 SUMMARY AND CONCLUSIONS

(i) Analysis of GMRT HI images indicates that UGC 4722 is a pair of merging dwarfs, as opposed to the interaction of a dwarf galaxy with a “dark” companion. The main galaxy has a rotational velocity $V_{\text{rot}} \sim 75 \text{ km s}^{-1}$. The smaller companion galaxy is almost completely disrupted making its rotation velocity hard to measure, our best estimate from the HI data is $V_{\text{rot}} \sim 35 \text{ km s}^{-1}$.

(ii) Analysis of H α P – V diagrams obtained with the slit positioned along the optical plume and the compact emission-line nebula on its edge, supports the conclusion that the nebula is an individual dwarf galaxy with a rotation velocity $V_{\text{rot}} \sim 40 \text{ km s}^{-1}$.

(iii) The combination of the optical photometry data, obtained from the SDSS images, with the estimates of the total HI fluxes derived from the GMRT HI-maps, reveals that both components are gas-rich, with $M(\text{HI})/L_B$ of 1.0 and 4.3, for UGC 4722 and the nebula ‘C’ plus plume, respectively.

(iv) A comparison of the plume colours with the PE-GASE2 model evolutionary tracks for instantaneous SFR shows that the colours are well matched by a stellar population produced in a single burst about ~0.5 Gyr ago. As suggested by statistical and numerical studies of starbursts in interacting galaxies we assign the time of the starburst to the peri-galactic passage of the companion.

(v) The oxygen abundance in the HII-regions in the two galaxies are 12+log(O/H)=7.64±0.06 (UGC 4722) and 7.50±0.10 (UGC 4722C). For both UGC 4722 and UGC 4722C the measured metallicity is substantially (i.e. a factor of 2–3) lower than that expected from the L–Z relation for similar luminosity galaxies in denser environments.

ACKNOWLEDGEMENTS

The authors thank A.V. Burenkov for help with BTA observations. SAP, DIM, YAP and ESS acknowledge the partial support of this work through RFBR grant No. 14-02-00520. DIM, IDK and SAP acknowledge partial support from RFBR grant No. 13-02-90407. JNC, IDK, SAP and DIM acknowledge the RFBR-Indian collaborative grant No. 13-02-92690. We acknowledge useful comments from the referee, N. Trentham, which have helped improve this paper. The authors acknowledge the photometric data and the related information available in the SDSS database used for this study. This research has made use of the NASA/IPAC Extragalactic Database (NED), which is operated by the Jet Propulsion Laboratory, California Institute of Technology, under contract with the National Aeronautics and Space Administration. This paper is based in part on observations taken with the GMRT. We thank the staff of the GMRT who made these observations possible. The GMRT is run by the National Centre for Radio Astrophysics of the Tata Institute of Fundamental Research

REFERENCES

- Abazajian K.N., Adelman-McCarthy J.K., Agüeros M.A., et al., 2009, *ApJS*, 182, 543
- Berg D.A., Skillman E.D., Marble A.R., et al., 2012, *ApJ*, 754, 98

- Briggs F.H., Möller O., Higdon J.L., Trentham N., Ramirez-Ruiz E., 2001, *A&A*, 380, 418
- Cannon J.M., Johnson M., McQuinn K., et al. 2014, *ApJ Lett*, 787, L1
- Chengalur J. N., 2013, NCRA Technical Report, NCRA/COM/001.
- Chengalur J.N., Pustilnik S.A., 2013, *MNRAS*, 428, 1579
- Chengalur J.N., Pustilnik S.A., Martin J.-M., Kniazev A.Y., 2006, *MNRAS*, 371, 1849
- Di Matteo P., Bournaud F., Martig M., Combes F., Melchior A.-L., Semelin B., 2008, *A&A*, 492, 31
- Ekta, Chengalur J.N., Pustilnik S.A., 2008, *MNRAS*, 391, 881
- Ekta B., Chengalur J.N., 2010, *MNRAS*, 406, 1238
- Fioc M. & Rocca-Volmerange B., 1999, *arXiv:astro-ph/9912179*
- Gottlöber S., Lokas E.L., Klypin A., Hoffman Y., 2003, *MNRAS*, 344, 715
- Hahn O., Carollo C.M., Porciani C., Dekel A., 2007, *MNRAS*, 381, 41
- Hahn O., Porciani C., Dekel A., Carollo C.M., 2009, *MNRAS*, 398, 1742
- Haynes M.P., Giovanelli R., Martin A., et al., 2011, *AJ*, 142, 170
- Hoeft M., Gottlöber S., 2010, *Advances in Astronomy*, v.2010, Article ID 693968, 16 pp.
- Hoeft M., Yepes G., Gottlöber S., Springel V., 2006, *MNRAS*, 371, 401
- Iyer M.G., Simpson C.E., 2006, *AJ*, 132, 1035
- Izotov Y.I., Thuan T.X., 2007, *ApJ*, 665, 1115
- Karachentsev I.D., Karachentseva V.E., Huchtmeier W.K., 2006, *A&A*, 451, 817
- Karachentsev I.D., Karachentseva V.E., Huchtmeier W.K., Makarov D.I., Kaisin S.S., 2008, in *Proc. of IAU Symposium 244 "Dark Galaxies and Lost Baryons"*, J.J. Davies and M.J. Disney, eds. p.235-246 = *arXiv/0708.1046*
- Karachentsev I. D., Makarov D. I., 2008, *AstBu*, 63, 299
- Karachentsev I.D., Makarov D.I., Karachentseva V.E., Melnyk O.V., 2011, *Astrophys. Bull.*, 66, 1
- Karachentseva V.E., 1973, *Comm.Spec.Ap.Obs. USSR Acad.Sci.*, 8, 1
- Kniazev A.Y., Grebel E.K., Pustilnik S.A., Pramskij A.G., Kniazeva T.F., Prada F., Harbeck D., 2004, *AJ*, 127, 704
- Kniazev A.Y., Zijlstra A., Grebel E.K. et al., 2008, *MNRAS*, 388, 1667
- Kreckel K., Joung M.R., Cen R., 2011, *ApJ*, 735, 132
- Kreckel K., Platen E., Aragon-Calvo M.A., van Gorkom J.H., van de Weygaert R., van der Hulst J.M., Beygu B., 2012, *AJ*, 144, 16
- Kroupa P., Tout C. A., Gilmore G., 1993, *MNRAS*, 262, 545
- Makarov D.I., Karachentsev I.D., 2009, *Astrophys. Bull.*, 64, 24
- Miskolczi A., Bomans D.J. & Dettmar R.-J., 2009, *A&A*, 536, A66
- Montuori M., Di Matteo P., Lehnert M.D., Combes F., Semelin B., 2010, *A&A*, 518, id.A56
- Patiri S.G., Prada F., Holtzman J., Klypin A., Betancort-Rijo J., 2006, *MNRAS*, 372, 1710
- Patton D.R., Torrey P., Ellison S.L., Mendel J.T., Scudder J.M., 2013, *MNRAS*, 433, L59
- Pilyugin L., Mattsson L., 2011, *MNRAS*, 412, 1145
- Peebles P.J.E., 2001, *ApJ*, 557, 459
- Perepelitsyna Y.A., Pustilnik S.A., Kniazev A.Y., 2014, *Astroph. Bull.*, 69, 247 (*arXiv:1408.0613*) (Paper IV)
- Pier J.R., Munn J.A., Hindsley R.B., et al., 2003, *AJ*, 125, 1559
- Prasad J., Chengalur J., 2012, *ExA*, 33, 157
- Pustilnik S.A., & Tepliakova A.L., 2011, *MNRAS*, 415, 1188 (Paper I)
- Pustilnik S., Zasov A., Kniazev A., Pramsky A., Ugryumov A., Burenkov A., 2003, *A&A*, 400, 841
- Pustilnik S.A., Kniazev A.Y., Pramskij A.G., 2005, *A&A*, 443, 91
- Pustilnik S.A., Tepliakova A.L., Kniazev A.Y., Martin J.-M., Burenkov A.N., 2010, 401, 333
- Pustilnik S.A., Tepliakova A.L., Kniazev A.Y., 2011, *Astroph. Bull.*, 66, 255 (*arXiv:1108.4850*) (Paper II)
- Pustilnik S.A., Martin J.-M., Tepliakova A.L., Kniazev A.Y., 2011, *MNRAS*, 417, 1335 (Paper III)
- Pustilnik S.A., Martin J.-M., Lyamina Y.A., Kniazev A.Y., 2013, *MNRAS*, 428, 1579
- Rojas R.R., Vogeley M.S., Hoyle F., Brinkmann J., 2005, *ApJ*, 624, 571
- Salpeter E. E., 1955, *ApJ*, 121, 161
- Schlafly E.F., & Finkbeiner D.P., 2011, *ApJ*, 737, 103
- Sorrentino G., Antonuccio-Delogu V., Rifatto A., 2006, *A&A*, 460, 673
- Tikhonov N.A., Galazutdinova O.A., Lebedev V.S., 2014, *Astron. Lett.* 40, 1
- Trentham N., Moller O., Ramirez-Ruiz E., 2001, *MNRAS*, 322, 658
- Tully R.B., Shaya E.J., Karachentsev I.D., Courtois H.M., Kocevski D.D., Rizzi L., Peel A., 2008, *ApJ*, 676, 184
- van den Bergh S., 1969, *Nature*, 224, 891
- Verdes-Montenegro L., Sulentic J., Lisenfeld U., Leon, S., Espada D., Garcia E., Sabater J., Verley S., 2005, *A&A*, 436, 443
- Walter F., Brinks E., 1999, *AJ*, 118, 273
- Wang J., Kauffmann G., Józsa G.I., et al. 2013, *MNRAS*, 433, 270
- Zasov A.V., Kniazev A.Yu., Pustilnik S.A., Pramsky A.G., Burenkov A.N., Ugryumov A.V., Martin J.-M., *A&AS*, 2000, 144, 429

This paper has been typeset from a \LaTeX file prepared by the author.